NEAR-SURFACE GEOPHYSICAL CHARACTERIZATION OF A HOLOCENE FAULT CONDUCIVE TO GEOTHERMAL FLOW NEAR PYRAMID LAKE, NEVADA

Alison Dorsey[1], Colton Dudley[1], John Louie[1], Paul Schwering[1], and Satish Pullammanappallil[2]
[1]Seismological Lab & Dept. of Geological Sciences & Engineering, University of Nevada, Reno, NV 89557 USA
[2]Optim, 200 S. Virginia St. Suite 560, Reno, NV 89501 USA

ABSTRACT

Linear deposits of calcium carbonate tufa columns mark recent faults that cut 11 ka Lake Lahontan sediments at Astor Pass, north of Pyramid Lake, Nevada. Throughout the Great Basin, faults appear to control the location of geothermal resources by providing pathways for fluid migration. Reservoir-depth (greater than 1 km) seismic imaging at Astor Pass reveals a fault that projects to one of the lines of tufa columns at the surface. The presence of the tufa deposits suggests this fault carried warm geothermal waters through the lakebed clay sediments in recent time. The warm fluids deposited the tufa when they hit cold Lake Lahontan water at the lakebed. Lake Lahontan covered this location 11 ka to a depth of at least 60 m. In collaboration with the Pyramid Lake Paiute Tribe, an Applied Geophysics class at UNR investigated the near-surface geophysical characteristics of this fault. The survey at and near the tufa columns comprises near-surface P-wave seismic reflection and refraction, electrical resistivity tomography, near-surface refraction microtremor arrays, nine near-surface direct-current resistivity soundings, magnetic surveys, and gravity surveys. The refraction microtremor results show shear velocities near tufa and faults to be marginally lower, compared to Vs away from the faults. Overall, the 30-m depth-averaged shear velocities are low, less than 300 m/s, consistent with the lakebed clay deposits. These results indicate that no seismically fast (> 500 m/s) tufa deposits are present below the surface at or near the tufa columns. Vs30 averages were for example 274 ± 13 m/s on the fault, 287 ± 2 m/s at 150 m east of the fault, and 290 ± 15 m/s at 150 m west of the fault. The P-velocity refraction optimization results similarly indicate a lack of high-velocity tufa buried below the surface in the Lahontan sediments, reinforcing the idea that all tufa was deposited above the lakebed surface. The seismic results provide a negative test of the hypothesis that deposition of the lakebeds in the Quaternary buried and preserved older tufa columns within the section. Near-surface Wenner arrays with a-spacings up to 30 m show a higher resistivity near the faults, and tufa, than away from the faults. Resistivity averages within a few meters of the surface were 33 ± 17 ohm-m on the fault, 13 ± 3 ohm-m east of the fault, and 9 ± 3 ohm-m west of the fault. It is possible that the geothermal waters are fresher, and more resistive, than waters held in the lakebed clays. Water samples from more than 1 km depth in exploration wells have a TDS of 2500 p.p.m., nearly drinking-water quality. The relatively resistive water, perhaps localized by greater permeability along the fault, could explain the higher resistivity measured near the fault. The results show that there is no high-velocity, high-resistivity tufa along the faults below the surface, so we are unable to use buried tufa to locate the faults that may promote geothermal upwelling in this area. We further hypothesize that as sedimentation buried the tufa during the Quaternary, warm geothermal waters re-dissolved it, and re-precipitated it in the cold lake-bottom water.

INTRODUCTION

The University of Nevada, Reno Applied Geophysics class conducted a geophysical survey in the Astor Pass area, near Pyramid Lake, Nevada to potentially locate geothermal resources. The Pyramid Lake basin is located within the Walker Lane Belt (WLB) system of northwest-striking right-lateral faults that generally parallel the eastern side of the Sierra Nevada mountain range. The WLB presently accounts for 15–25% of the motion between the North American and Pacific Plates (Thatcher et al., 1999). The northwest-striking, right-lateral Pyramid Lake fault extends southward more than 45 km and shows evidence of at least four different earthquake events in the past 15 ka (Briggs & Wesnousky, 2004). Association of the northern WLB with the Pyramid Lake basin promotes crustal dilation and deeper penetration of fluids along these steeply dipping faults (Faulds et al., 2005). This structural relationship enables increases in higher local heat flux and, therefore, increased potential for geothermal energy production (Faulds et al., 2005).

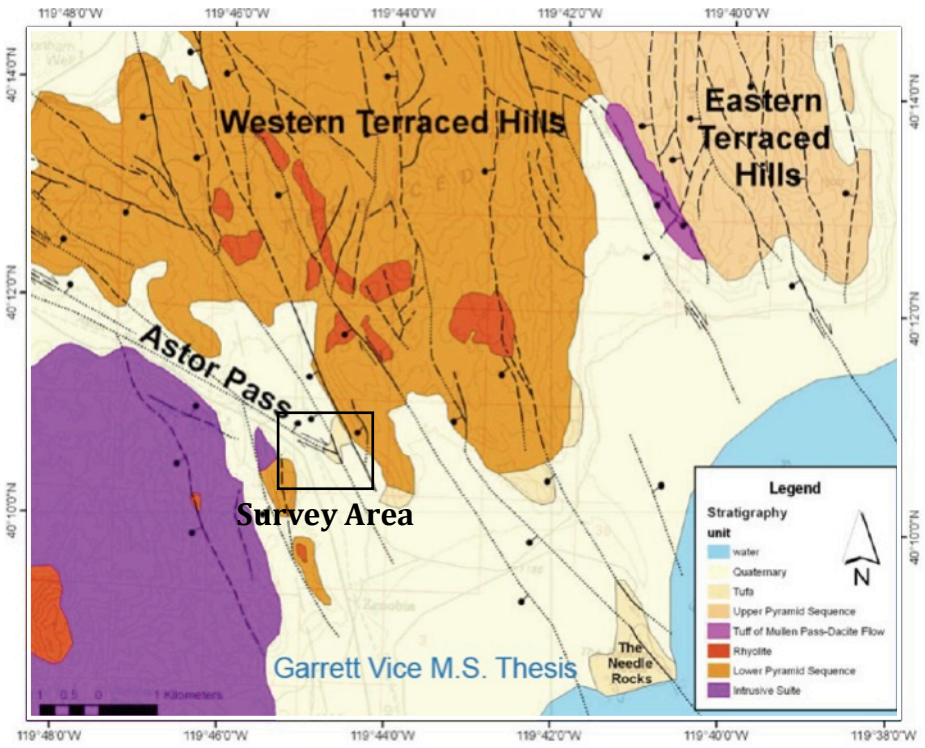

Figure 1. Location map showing the Astor Pass survey area. The Astor Pass geothermal system lies at the terminus of the Pyramid Lake fault zone, a transitional region between northwest-trending dextral shear in the Walker Lane and north-northeast striking normal faults in the northern Basin and Range province (Vice, 2008).

A case study suggests that geothermal resources exist in Astor Pass. To test this hypothesis, they employed remote sensing data sets to obtain hydrothermal alteration maps. Even though they were unsuccessful in obtaining a geothermal well, this study helped guide geothermal exploration at Astor Pass with regional-scale mineral mapping that focused subsequent exploration efforts. Furthermore, the results provide examples of how altered rock and certain chemical precipitates used as geothermal exploration guides.

This study comprises near-surface seismic reflection and refraction, electrical resistivity tomography, nine near-surface refraction microtremor arrays, nine near-surface direct-current resistivity soundings, magnetic surveys, and gravity surveys. The focus of the survey is to locate a geothermal system near a set of tufa spires. The setting at Astor Pass suggests that tufa towers are promising indicators for blind geothermal systems (Vice, 2008). Promising features for future exploration include multiple structurally controlled linear tufa towers, intersecting faults, and kinematic data suggestive of pull-apart zones or dilation at the fault intersection (Vice, 2008). The goal of this study is to localize the geothermal system by identifying regional anomalies, designing structural-specific seismic surveying, and interpreting seismic profiles to determine the direction of dip for such a fault, or faults.

METHODS

Near-surface seismic reflection and refraction, electrical resistivity tomography, near-surface refraction microtremor arrays, nine near-surface direct-current resistivity soundings, magnetic surveys, and gravity surveys were utilized to fulfill our objectives. Measurement points were surveyed with an EDM theodolite, providing locations for all of the geophysical surveys.

Seismic Reflection and Refraction

The near-surface seismic reflection and refraction survey utilized a seismic cable connected to a 48-channel Bison recorder, 3 m takeout spacing, and six 100-Hz geophones in groups laid parallel along each of the two contiguous lines on the NW-SE sides of the tufa tower with a line aperture of -280 m. Hitting a 7 kg sledgehammer against a steel plate ten times simulated Wave propagation.

Seismic processing included Dr. John Louie's JRG seismic processing system. Geometry was applied to both seismic line datasets. Each data set compromised of filtering, picking first seismic wave arrivals, stacking, and migrating data to achieve a stratigraphic cross section of each seismic line. First seismic wave arrivals were processed by SeisOpt® ReMi™, © 2012 Optim for a color contour gridded velocity section of each seismic line in order to confirm accurate seismic data processing.

Electrical Resistivity Tomography

Multi-Phase Technologies collected a 292 m northeast-southwest trending survey line south of the tufa spire alongside the seismic reflection/refraction line. The survey was collected in two separate sections. Section 1 was centered over the suspected tufa fault, containing 64 electrodes with 3 m spacing. While section 2 was created by starting at the end of section 1 and rolling 32 of the 64 electrodes to the west. The "roll along" survey produced overlapping data points over the suspected fault area, which yielded better resolution.

The maximum length of 195 m per section allowed for a maximum depth penetration of approximately 33 m. Overall, MPT collected more than 10,000 data points, resistivity and induced polarization (IP), using MPT's field Data Acquisition System (DAS-1) unit.

A traditional ERT dipole-dipole array and an ERT pole-dipole array were utilized to collect data. The traditional dipole-dipole data yielded noisy results, which occurred on pairs when the transmitter dipole distance was small and space separating the dipoles was large. The pole-dipole array, however, increased the signal to noise ratio and depth penetration of the array. In order to collect pole-dipole data, the pole electrode was placed 130 m east of the initial start of the electrode line. All of the ERT data discussed in this report were collected in time-domain induced polarization mode at base frequency of 1 Hz. The IP data used a 100 millisecond measurement window centered 150 milliseconds after the turnoff.

In order to process the data, an IP filter was placed on the pole-dipole data set. The filter removed any data points that had chargeability values greater than 50 mV/V or less than -50 mV/V, respectively. In addition to an IP filter, a reciprocal filter was applied to the dipole-dipole data, which interchanged the locations of the receiving and transmitting electrodes. The reciprocal filter acts as a check on data accuracy since the "normal" and reciprocal measurements are supposed to have the same values. If the percent difference was greater than 5%, the two data points were removed and were not used during the inversion process. Reciprocal measurements were not performed on the pole-dipole data because the pole-dipole method uses dissimilar transmitters (i.e. the pole) and receivers (i.e. the dipole) that do not lend themselves to reciprocal measurements. All of the pole-dipole data used a single reference electrode located east-northeast of the survey line.

Refraction Microtremor

The refraction microtremor method was utilized to collect Rayleigh wave data and calculate shear wave velocities for site classification purposes. A combination of North-South and East-West trending lines of data were collected in Astor Pass. The Northeast-Southwest lines crossed the tufa spire at the midpoints to locate a hypothesized fault.

The Bison seismograph was employed as the data-receiving unit to collect and save data. Twelve vertical geophones were attached and leveled at 10 m increments to the 110 m long array, which was connected to the seismograph (through the "Y" cable). Each vertical geophone worked at 4.5 Hertz. To create noise, a truck was driven back and forth along the array of geophones. Overall, approximately ten sets of data for each array line was collected.

To process the data, P-F plots were filtered and combined for all data sets recorded from the same line location using SeisOpt® ReMi™, © 2012 Optim. If a plot appeared to be damaged, it was not included in the combined P-F plot. Minimum velocity picks were made and saved. Using ReMiDisper®, velocity estimates and layer depths were created. By plotting these results with Google Earth, it was possible to analyze the data with respect to position. Separate P-F plots for these traces were created, picked, and analyzed.

Resistivity

For resistivity, electrodes were placed in the ground at given a-spacing distances, 6 to 11 m apart. A Wenner array formation consisted of outer electrodes carrying the electrical current and inner electrodes carrying the electric potential. Two Wenner arrays constituted one line, with the final apparatus displaying the following lineup: current (+), potential (+), resistivity meter,

potential (-), current (-). The lines were placed on the same lines conducted by the ReMi technique, around the fault zones. Once the line contained a secure connection into the ground, a resistivity meter then recorded current in Ω or mΩ and the Induced Polarization (IP) value. For each reading the a-spacing distances decreased from 11 to 6 meters. The resulting apparent resistivity, the average resistivity influencing the current, derives from the recorded records.

Magnetic Survey

Magnetic data collected in the Astor Pass geothermal prospect area, used one roving Scintrex magnetometer, and another stationary Scintrex magnetometer as the base station. The base station measures diurnal variation of the Earth's magnetic field to remove this variation from the rover data, and to provide an average value for the base-level magnetic field for the survey. The rover took readings at locations of about 50 meters but tightened to as small as 5 meters in areas that indicated anomalies. Survey control utilized NAD83 UTM Zone 11N metric coordinates, established by hand-held GPS units. The base station magnetometer collected 30-second time sampling data for the entire duration of the survey – about 27 hours. The calculated base field measured about 50728.4 nT.

Magnetic data processing was conducted with Geosoft's Oasis Montaj. Magnetic mobile, base, and GPS datasets were imported and cross-correlated for correction and total magnetic intensity profiling. A total magnetic field color contour map was gridded and plotted entailing regional Astor Pass structural properties.

Gravity Survey

The Gravity team collected the gravity data using the Lacoste and Romburg model G gravimeter. Since the number of readings depends on the accuracy of each reading, two to three readings were made at each gravity station, lifting and re-leveling the gravimeter each time. In order to keep the readings consistent and accurate, the gravimeter remained plugged into a battery and the gravimeter's temperature was periodically checked.

The relative elevations and locations of each gravity station were measured using the laser Theodolite coupled with a rod at each location. The Theodolite remained at a fixed location each day, with the coordinates recorded. Any adjustments to the rod heights or battery changes were recorded as well.

Once a simple Bouguer anomaly calculation and B and C ring terrain corrections were made, the Gravity data was processed using GeoSoft software, Oasis Montaj and GM-SYS. The terrain corrections were estimated by eye; using hammer zones from 0-50 ft and 50-150 ft distances within zones B and C.

The gravity survey included 26 measurements with a set base station at UNR in the SEM building. In order to put all of the data into GeoSoft, the loop closures were labeled among the other flags with their own "flag numbers," A1, A6, AA7, etc., with each day having a separate spreadsheets. Furthermore, the base stations at UNR in the SEM building were inputted as separate spreadsheets with the labels SEM followed by the date that each reading was taken.

It was later decided that additional gravity data filling in the areas to the north and south of the E-W trending profile line would be beneficial in providing a broader interpretation of the area. This secondary survey was conducted on 11/20/2013 using the same Lacoste and Romburg model G gravimeter as the previous survey team.

Data were collected at 14 more points using the same methods as previously described; taking 3 readings, picking up and re-leveling the gravimeter each time. The same base stations at UNR and at the survey location were used as in the previous survey. Relative elevations were collected in the same way as well, using a laser theodolite with a height adjustable rod and inclinometer. The Theodolite had to be moved several times to points in which the elevations had been measured in order to provide line of sight to the next point.

The data from this survey was reduced in Excel using the methods outlined in Telford et al. (1989). The inner B and C terrain corrections were estimated by eye using the same hammer zone distances as previously described. The outer terrain corrections were calculated using software developed by Donald Plouff of the U.S.G.S. (http://www.geopotential.com/docs/OuterTC.com)

The data from both surveys were then integrated and the complete Bouguer anomalies for both sets of data are shown in fig. 15. Data from the previous survey is labeled A1, A2, A3… and data from the secondary survey is labeled 1, 2, 3… The data from the second survey also includes a measurement at a U.S.G.S. section corner labeled "SC".

RESULTS

The seismic reflection and refraction, electrical resistivity tomography, refraction microtremor arrays, direct-current resistivity soundings, magnetic surveys, and gravity surveys successfully gathered the necessary information to provide accurate results. The overall result of the data suggests that the large tufa spire is solely aboveground, with the possible presence of a normal fault dipping west along the tufa mounds and a left dip-slip fault in the east.

Time distance plots helped calculate velocities V_1 and V_2 that were used in the minimum and maximum depth calculations (time-distance plot is shown in Figure 2). The V_1 velocity ranged from 275 m/s to 400 m/s, with an average of 337.5 m/s. The V_2 average velocity was about 1090 m/s. The depth of the first refractor was between 15-30 m. The apparent refractor dip was between 1 and 5 degrees. Using the reverse shot data, an intermediate layer did appear present; however, this third layer could have been from noise while collecting the data and was not apparent on the forward shot. The maximum structural defection depth calculated was 5.3 m.

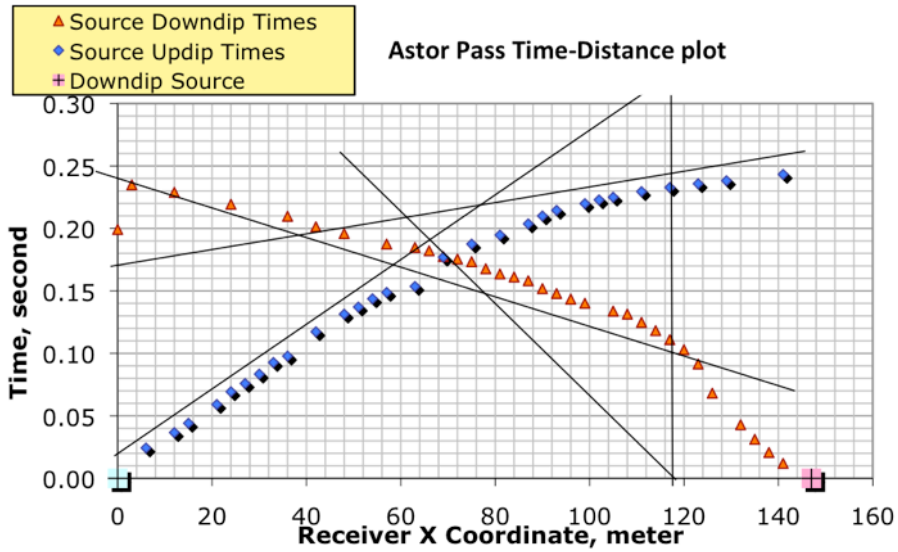

Figure 2. A Time-Distance plot showing the apparent velocities of the Astor Pass refraction data.

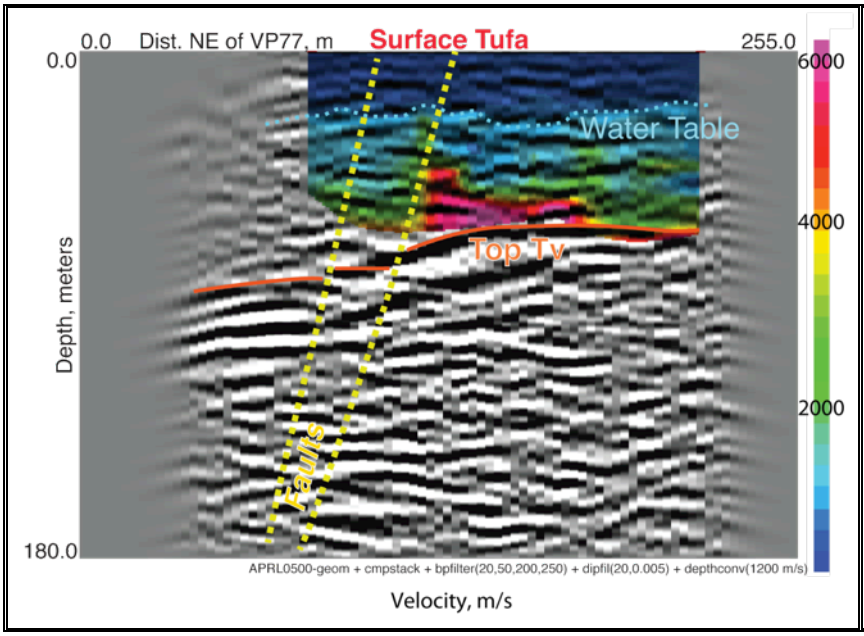

Figure 3. An interpretation of velocity overlaying the seismic image. We hypothesize that the high velocity area represents sinter, tufa, or Tertiary volcanics.

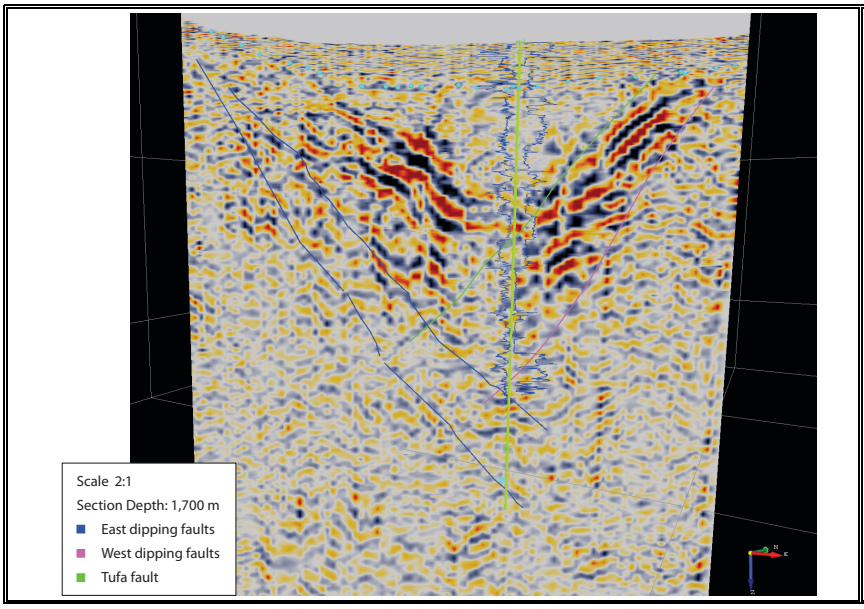

Figure 4. Deep seismic (5,600 ft/1,700 m) south of tufa spire showing reflective tertiary basalts as well as east and west dipping faults. AP3 well with sonic log on left and gamma log on right. The section is north looking toward Pyramid Lake.

Figure 5. Location map of the ERT line and the Seismic Reflection and Refraction line near the main tufa column.

Multi-Phase Technologies' ERT results allow for another analysis the seismic data. Once the data sets were filtered, the dipole-dipole and the pole-dipole data were merged together into one data file. Overall, the pole-dipole data had higher signal levels for the long transmitter-to-receiver separation that provide deeper penetration. However, the dipole-dipole data showed better resolution of the shallow structure and the combined dipole-dipole and pole-dipole data sets appear to provide the best overall results.

Sections 1 and 2 both show a conductive layer at a depth of 10-15 m. In Figure 6B, the conductive (blue) layer starts to fade around a distance of 120 m and disappears entirely east of 110 m. However, from Figure 6A, we can see that the layer is continuous to a distance of at least 70 m. This comparison with the right (west) side of Figure 6A with Figure 6B is a bit more complicated since the strength of the anomaly does start to fade in Figure 6B around a distance of 150 m. It appears that this layer is imaged to within about 20 m of the end of the survey. The conclusion is that the layer is discontinuous on the east side of the survey since it disappears well before this 20 m limit in Figure 6A. It is also probably discontinuous on the west side of the survey.

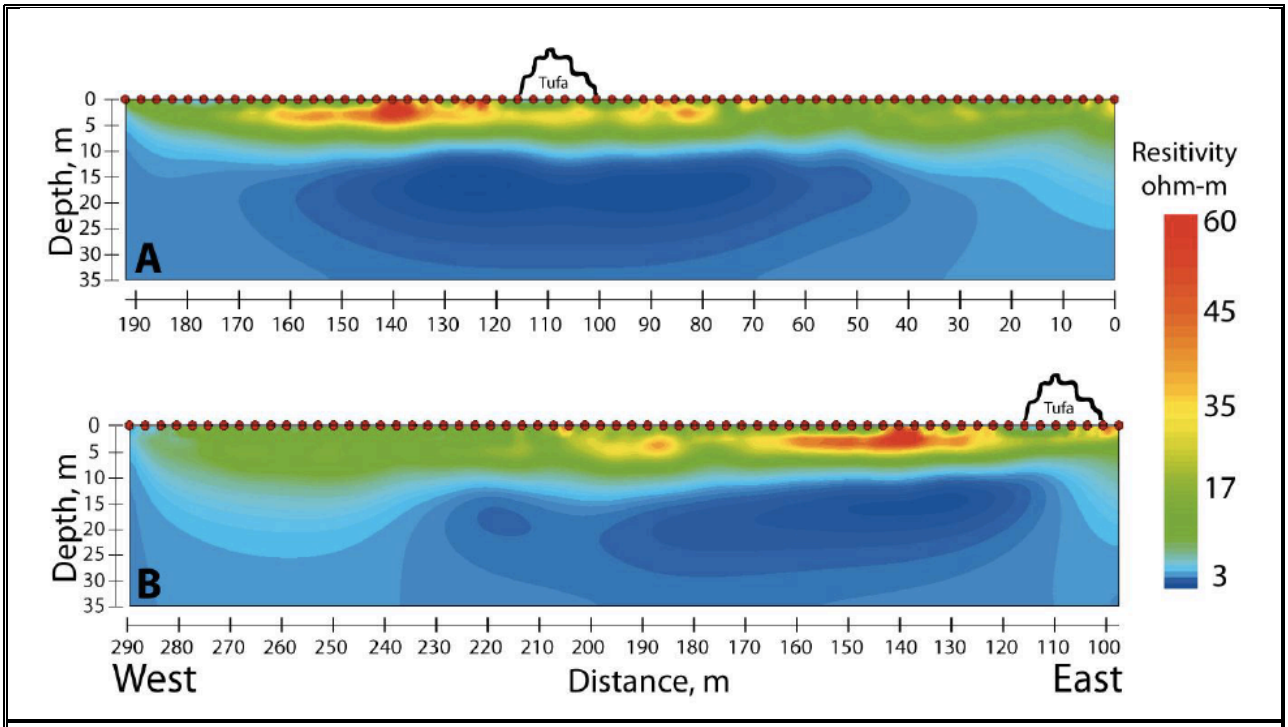

Figure 6. The results of the individual sections looking north, A) Section 1, the most eastern section. B) Section 2, the most western section, note that the conductive layer appears to end at 240 m west.

Figure 7 shows the inversion results after combining both sections into a single 290 m line. Interpreting the two sections as a single, comprehensive data set provides improved resolution of the entire line. In Figure 7, there is no resistivity signature indicating that the tufa extends below the surface. The conductive layer appears relatively flat. As discussed previously, the layer is probably does not continue eastward. A large gap in the conductive layer occurs at a distance of 180 m and a smaller gap east of the tufa.

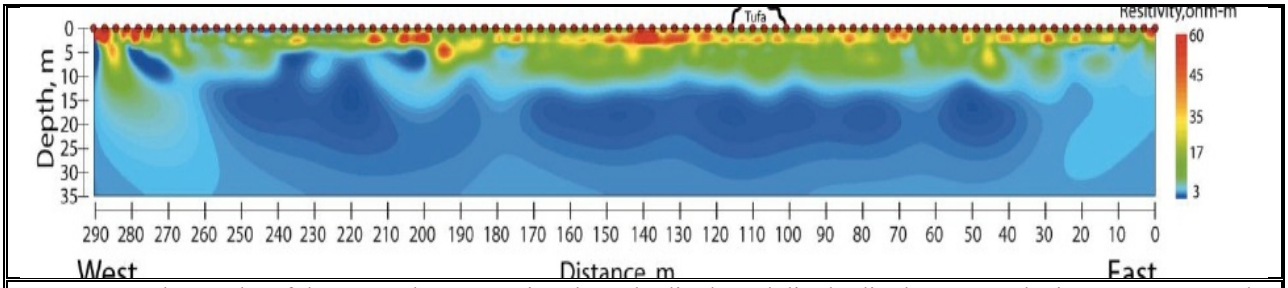

Figure 7. The results of the merged survey using the pole-dipole and dipole-dipole arrays. The image was created using a -50 to 50 IP filter on the pole-dipole data and a 5% reciprocal filter on the dipole-dipole data.

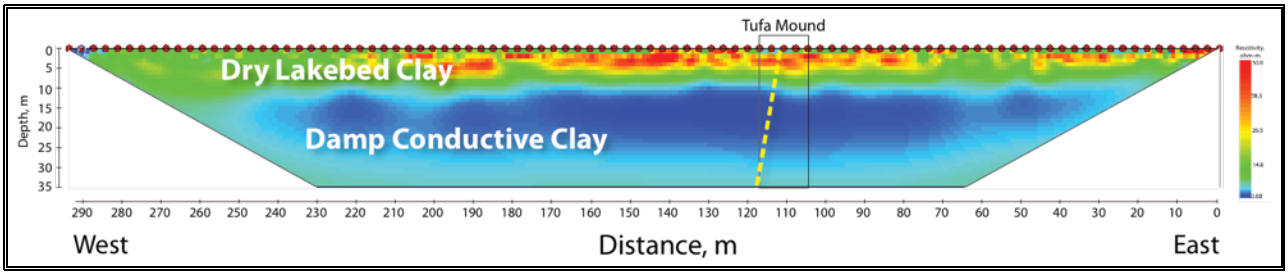

Figure 8. ERT showing dry lakebed clay near the surface and damp conductive clay below. The hypothesized tufa fault is represented with the yellow line.

Further analysis of the Astor Pass refraction data was completed using SeisOpt® ReMi™, © 2012 Optim. The results are shown below in Figure 9.

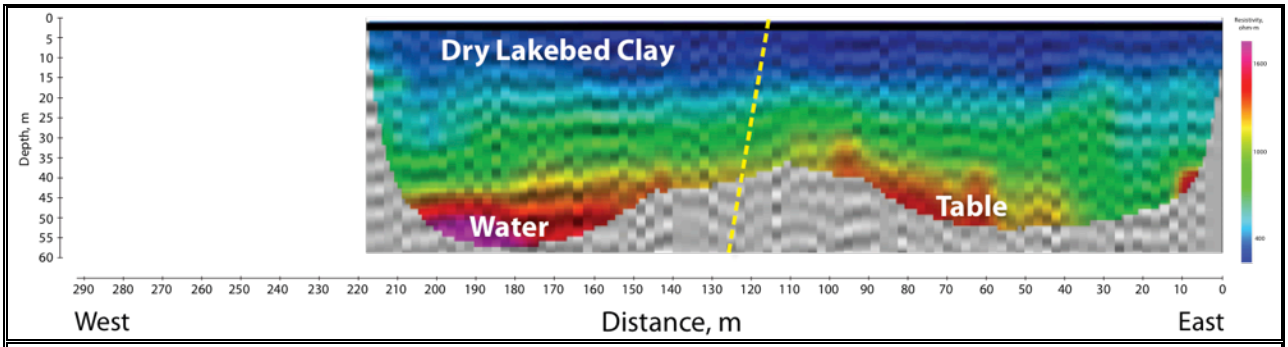

Figure 9. Seismic refraction overlayed on top of seismic reflection showing dry lakebed clay near the surface and the water table below. The hypothesized tufa fault is represented with the yellow line.

P-wave velocities are consistent with the simple calculations of 275-400 m/s, with refraction microtremor results showing a surface velocity between 300 and 400 m/s. The estimation of the refractor depth being between 15 and 30 m is also consistent with Refraction microtremor results, pointing at a first refractor depth of 12-16 m.

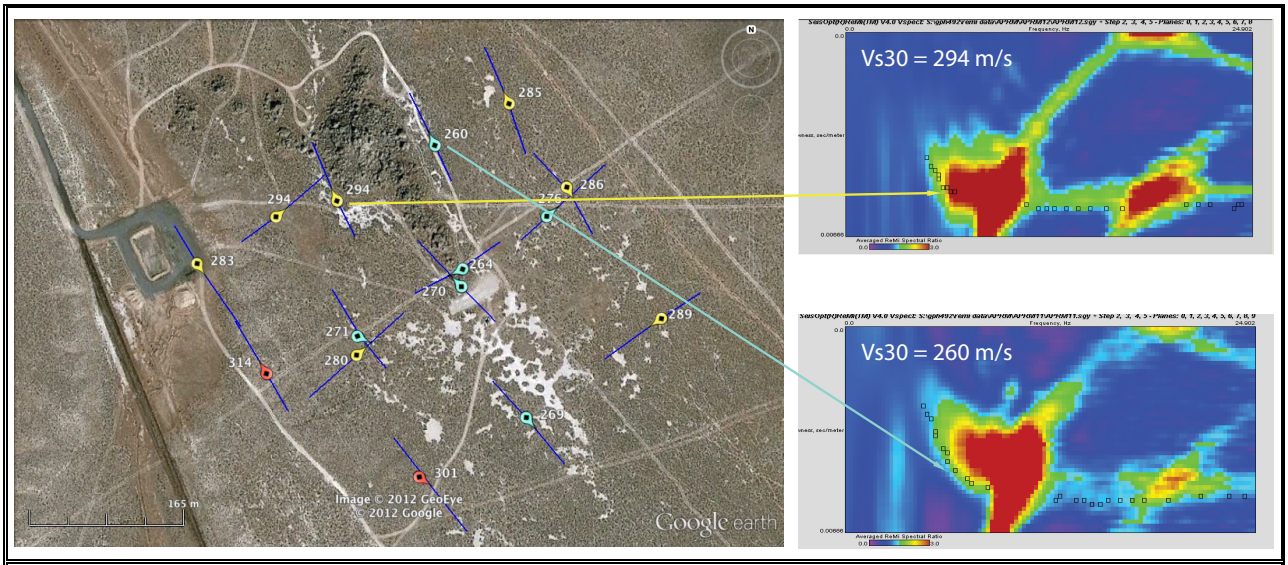

Figure 10. Map of Vs30 arrays, with values in m/s. Note the arrays atop the tufa fault give marginally lower Vs30 than the arrays away from the tufa. Overall there is a possible 10% decrease in Vs30 at the Tufa Fault.

Results from Refraction microtremor did not agree with the hypothesis of seeing faster velocities near the middle of the plot where tufa bodies were thought to exist. These results actually lean towards a hypothesis that most, if not all, of the Tufa is on the surface.

There were strong winds and other sources of noise on the seismic line while collecting data. These sources of error could produce slight inconsistencies in the data, but high-velocity tufa bodies should have produced notably earlier first-arrival times. Picks of the first arrival times were difficult to see in sections; however, the results were consistent throughout the entire plot, suggesting a few wrong picks would not have thrown off the whole data set.

Cvstacking generated very few continuous reflections. This is most likely a result of the wavy, inconsistent presence of reflections on each plane. Based on a fairly common and expected velocity of 1,200 m/s one reflector was identified. Based on that velocity and its two-way travel time its depth was 120 m. This is generally consistent with the drilled depth to the Tertiary volcanic section 90-150 m deep. The cvstack is depicted in Figure 11.

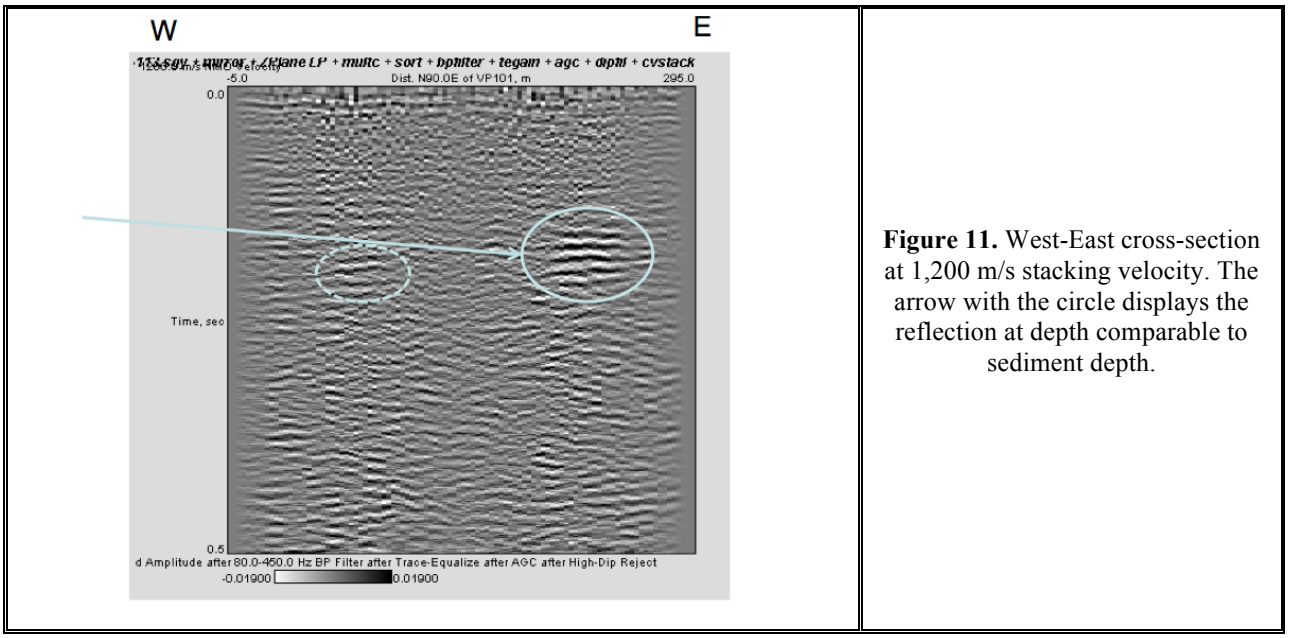

Figure 11. West-East cross-section at 1,200 m/s stacking velocity. The arrow with the circle displays the reflection at depth comparable to sediment depth.

The cmpstack is based roughly on the refraction results. This does not work well, especially since NMO-velocities are needed to stack and refraction results are loosely analogous to Dix interval velocities.

The low velocity trend seen near the tufa spire shows the exact opposite result than expected. The reason for this could be that the vibrations picked up in the refraction microtremor data were almost completely reflected by the higher velocity tufa layer. Immediately around the tufa spire, the data shows faint traces of a higher velocity layer. This trace shows velocities for the high velocity layer around 1300 m/s, compared to the 400-500 m/s velocities seen in the main track (Figure 12). The faint traces were only seen strongly in data from lines 11 and 12. There were very faint traces in lines 4,6, and 8, but they were not strong enough to make picks.

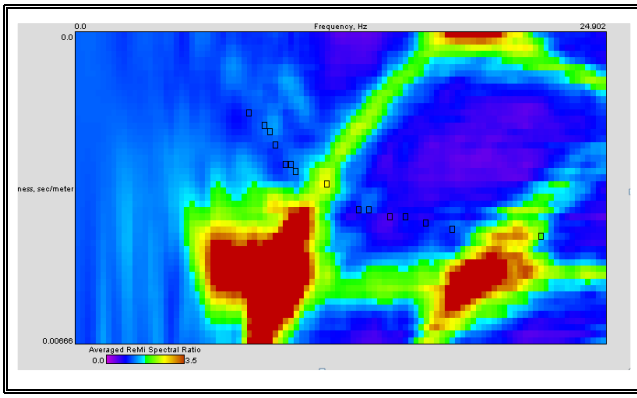

Figure 12. The faint higher velocity trace is picked above. The velocity of this layer is 1300 m/s.

The depth to layer results did not show as much correlation as the velocity results; however, the depths were fairly constant around the spire (± 0.75 m). The depths not immediately surrounding the spire varied greatly (± 11 m).

Although there is a chance for experimental error, such as unleveled geophones, the tufa spire appears to increase in depth slightly faster to the east.
The resistivity data at Astor Pass shows, immediately on/near the tufa tower, a jump in resistivity in the larger a-spacings (Figure 14). This indication exists among the E-W readings, showing that lines 148 or 160 have a higher than average resistivity, especially in the 6-11 m spacing. Within this a-spacing region, there exists a resistance interaction with the tufa and low porosity/water content near the tufa spire.

Almost all trends show that by the 27 m a-spacing, all resistivity drops below 10 ohm-m, which corresponds to water content in the subsurface. There are a few anomalies to this conclusion, however, such as “101-A (N-S)” and “148 C (N-S)”. For “101 A (N-S)” it may be dryer than the surrounding area. On the other hand, the “148 C (N-S)” was right alongside of the largest part of the tufa mound, which due to the high resistivity throughout the line, can conclude to have an effect due to the tufa, extending down to the 27 m A-space depth.

The north/south line resulting plots, shows that there exists a relatively low resistivity with depth on the east and west sides of the tufa -- Q type graphs. At the tufa itself there contains a higher resistivity reading indicating the presence of the tufa. The east/west graphs all show that a Q type exists on either side of the mid line chart, which represented the 148 and 160 m marks. Therefore, the resistivity expresses that the tufa comprises of a linear body in the subsurface trending along the 148 m line.

Figure 13. Location map of the resistivity soundings. The Q-Type profiles are located along the tufa fault, while the K-Type profiles are located away from the fault.

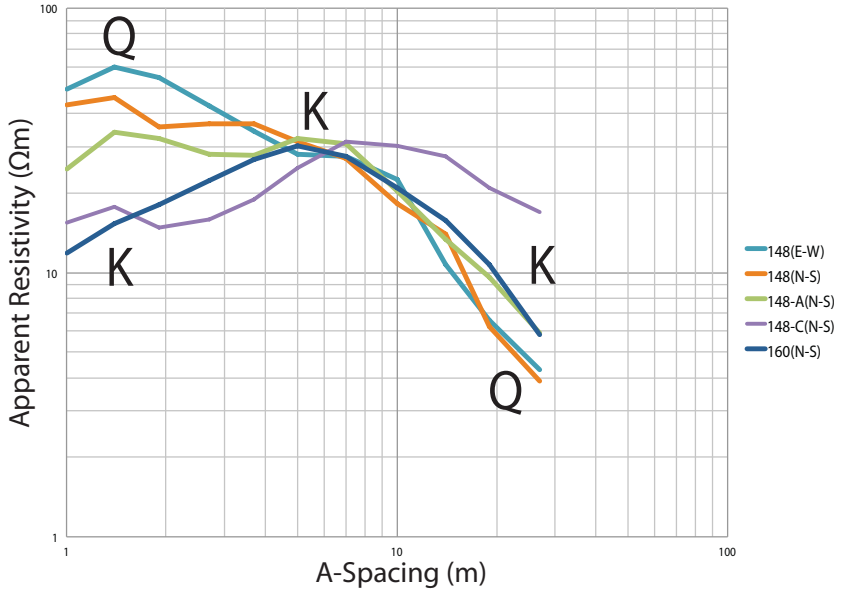

Figure 14. A graph of the apparent resistivity with respect to the a-spacing.

To obtain reasonable results for the gravity data, a single E-W trending profile line (Figure 15) was chosen as the best fit for highlighting a WNW dip/slip fault from previous studies.

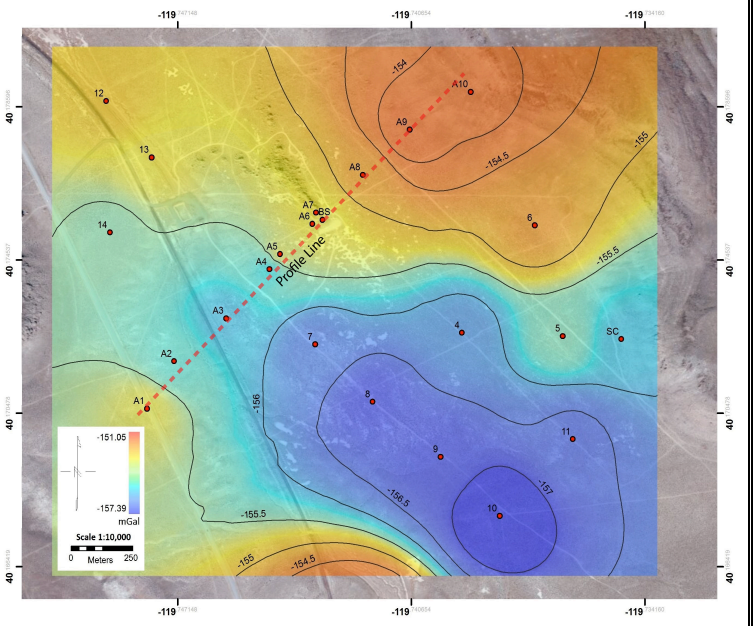

Figure 15. Complete Bouguer anomaly showing the chosen profile line.

A profile of the complete Bouguer anomaly (Figure 16) is displayed from west to east (right to left), with an overall increasing trend. It is important to note that there is a very small change in gravity and magnetic values across the profile.

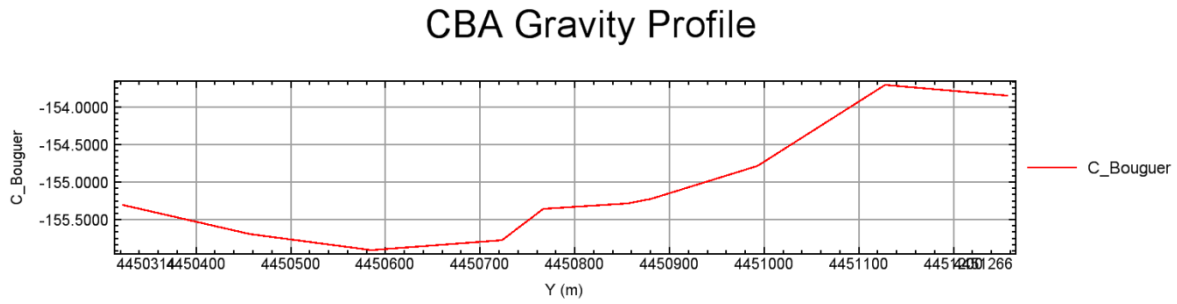

Figure 16. The profile of the complete Bouguer anomaly, displayed from west to east.

The magnetic profiles show 7 north-east to south-west trending lines, which indicate decreasing magnetic values projecting along the strike of an eastern edge of the central tufa spire (Figure 17).

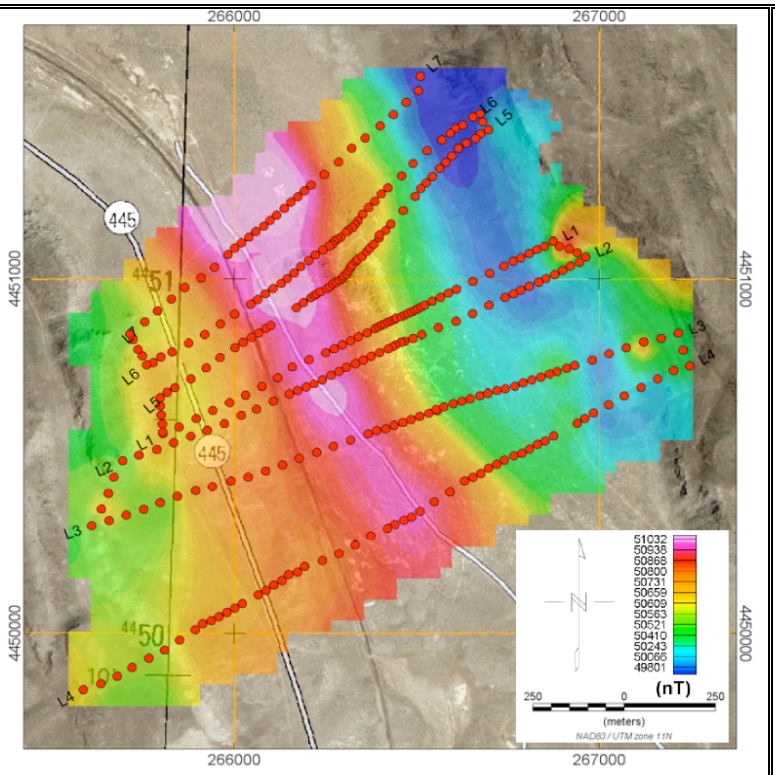

Figure 17. The red dots represent the location of the magnetic rover stations. Each of the 7 major transect (WSW-ENE orientation) roughly extends a mile long. Nominal station spacing extended 50 meters, but tightened to as little as 10 meters in areas of high observed magnetic gradient. Tufa fault appears to bound the east side of the strong anomaly.

The gridded color contour map of the corrected total magnetic field measurements of the rover show a perpendicular-to-line trend of magnetic features, with a steady increase in magnetics from the western range-front towards the central tufa. The volcanics on the eastern range-front result in noisier readings.

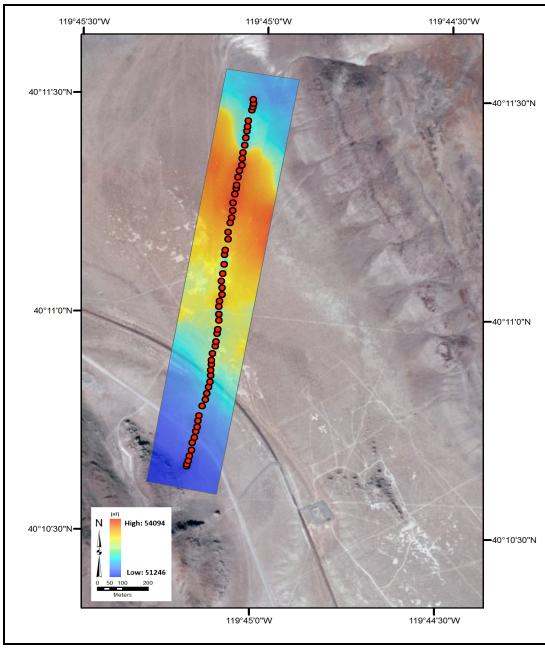

Figure 17.b The points in this figure represent another magnetics line to the north of the original survey area, which can be seen in the lower right of the map.

The data was collected using a magnetometer built into the iPhone 3GS. Although the range of the data is different from that collected by the Scintrex magnetometer, similar trends in magnetic anomalies can be seen when compared to the data in figure 17.

Profiles for the connecting lines are not included in the profile map since none show significant character in profile; however, these measurements exist in the gridding. Gridded magnetic data range from about 1200nT and indicated a steady increase in magnetic field from the western range-front towards the central tufa, peaking on the west side of the tufa mound where drilling occurred, and then a decrease from the tufa eastward towards the eastern range-front (Figure 17). The volcanic deposits on the eastern range-front resulted in noisier readings. This suggests a normal fault dipping west may be present along the tufa mounds. However, in the eastern region of low magnetic readings, there presents a possible left dip-slip fault. According to previous records, a strike-slip fault stops just before the range front. This result may indicate that the fault actually extends further, pass the normal fault associated with the tufa mound. Figure 17.b shows a secondary magnetics line collected using an iPhone magnetometer. Although the reading values have different ranges similar trends in anomalies can be seen moving from the western to eastern range fronts.

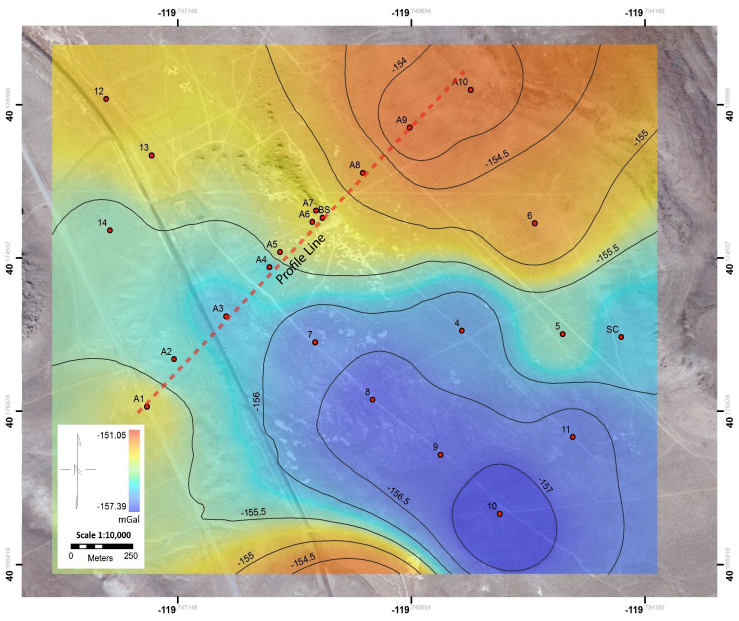

Figure 18. The Complete Bouguer anomaly color contour map results.
The modeled Profile line is highlighted.

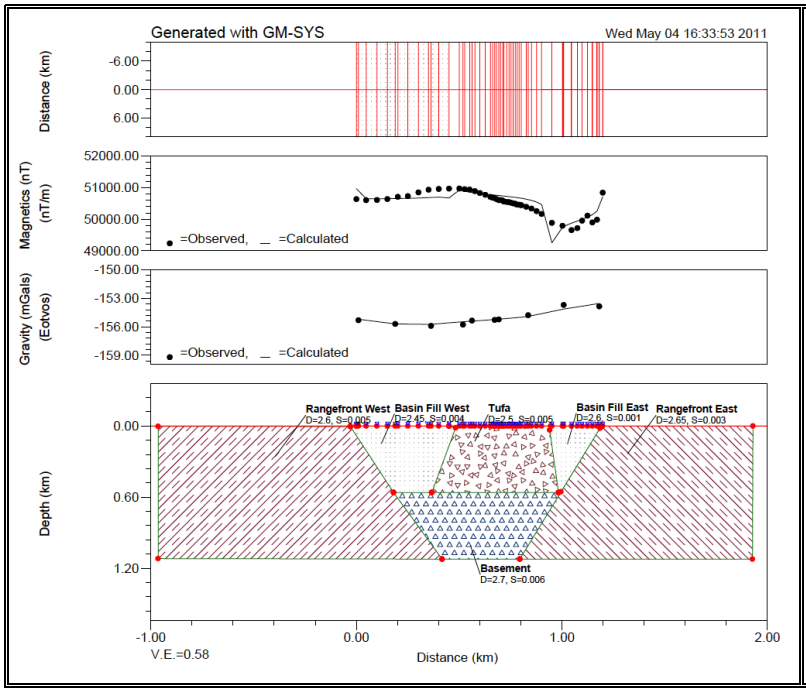

Figure 19. The final geologic model, which was created using L1 of the magnetic data and the profile line of the gravity data.

DISCUSSION

Astor Pass is an increasingly popular location for geothermal exploration. The studies mentioned in the introduction (Thatcher et al., 1999, Briggs & Wesnousky, 2004, Faulds et al., 2005, Kratt et al., 2010, Vice, 2008) justify this theory, making it an ideal location to continue the exploration. While these studies identify the fact that there is a possible resource somewhere beneath the Astor Pass soil, none of them actually prove it. They do, however, provide the necessary framework, that allowed us to discover some interesting features. While we remain in the dark about the precise whereabouts of any geothermal, we successfully determined that the regional magnetics show an anomaly that coincides with the tufa fault orientation and regional gravity data show an anomaly that coincides with the WNW oblique-slip fault. Furthermore, surface resistivity values are three times higher near the fault than away from the fault and ReMi arrays show a max 10% decrease in Vs30 across the tufa fault. Additionally, shallow reflection/refraction show no tufa below the surface, but a possible sinter deposit above the Tertiary volcanics. According to a previous study by Jim Faulds (2005) a strike-slip fault stops just before the range front. Our results may indicate that the fault actually extends further, past the normal fault

associated with the tufa mound. This very observation may represent the key in finding a geothermal well, with the Eastern intersection of the range-front and tufa being the target.

Furthermore, the geology of this section is thought to be dry clay at the surface, followed by a layer of moist sand or better-graded sand and clay in the middle, and water-saturated sand and clay at ~40 m depth. With Astor Pass at about 1219 m elevation and Pyramid Lake at ~1156 m, a water-table elevation of ~1180 m seems reasonable, with a Tertiary volcanics elevation of ~1120 m. Tufa spires above the surface are located in the middle of the plot at 150 m distance, but do not show any signs of higher velocities (>2000 m/s) below the surface, with results showing that most, if not all, of the tufa is on the surface. One hypothesis as to how this may have occurred is that this particular tufa mound formed directly around a large plant. The only skeptical notion is how this large plant grew underwater in the first place. Overall, this discovery represents a step forward in characterizing the geothermal resources by identifying structures at the top of the Tertiary volcanics.

ACKNOWLEDGEMENTS

This material is based upon work partially supported by the Pyramid Lake Paiute Tribe; and the U.S. Dept. of the Interior, Division of Energy and Mineral Development, Office of Indian Energy and Economic Development; with additional work partially supported by the U.S. Department of Energy from DE-FOA-0000109 Recovery Act: Geothermal Technologies Program, and under instruments numbered DE-FG07-02ID14311 and DE-FG36-02ID14311, managed through the DOE Golden Field Office.

Acquisition of additional gravity data conducted by Marlon Ramos and Dustin Naphan.

REFERENCES

Anderson, R. Ernest, compiler, 1999, Fault number 1118, California Wash fault, in Quaternary fault and fold database of the United States: U.S. Geological Survey website, http://earthquakes.usgs.gov/regional/qfaults, accessed 05/06/2011 11:43 AM.

Briggs and Wesnousky, 2004 R.W. Briggs and S.G. Wesnousky, Late Pleistocene fault slip rate, earthquake recurrence, and recency slip along the Pyramid Lake fault zone, northern Walker Lane, United States, *Journal of Geophysical Research* **109** (2004), p. 16.

Cosatt, 2009 Matt Cosatt, Preliminary Gravity Analysis of the Crustal Structure Within the Tendaho Graben and Manda Hararo Rift in the Central Afar, Ethiopia, *The Geological Society of America* (2009).

Faulds et al., 2005 J.E. Faulds, C.D. Henry and N.H. Hinz, Kinematics of the northern Walker Lane; an incipient transform fault along the Pacific-North American Plate boundary, *Geology* **33** (6) (2005), pp. 505–508.

Kratt et al., 2010 Christopher Kratt, Wendy M. Calvin and Mark F. Coolbaugh, Mineral mapping in the Pyramid Lake basin: Hydrothermal alteration, chemical precipitates and geothermal energy potential, United States, *Remote Sensing of Environment* **114** (2010), pp. 2297-2304.

Multi-Phase Technologies, LLC. Electrical Resistivity Tomography Survey Astor Pass Geothermal Site, Pyramid Lake, Nevada September 2012. Tech. Print.

Taylor et al., 2001 Taylor, W. J., Criscione, J. J., Gilbert, J. J., Justet, L., Kula, J. L., Schiefelbein, I. M., Sheely, J. C., And Stickney, E. K, Geometry and Neotectonics of the northern California Wash fault, southern Nevada, United States, Geoscience, UNLV (2001).

Telford W.M. , Geldart L.P. , Sheriff R.E. , (1990). Applied Geophysics, Second Edition Cambridge University Press. New York.

Thatcher et al., 1999 W. Thatcher, G.R. Foulger, B.R. Julian, J. Svarc, E. Quilty and G.W. Bawden, Present-day deformation across the Basin and Range province, western United States, *Science* **283** (1999), pp. 1714–1718.

Vice, Garret S., 2008 Structural controls of the Astor Pass-Terraced Hills geothermal system in a region of strain transfer in the western Great Basin, northwestern Nevada, *University of Nevada, Reno* **1456425** (2008), p. 128.

Zaragoza et al., 2005 Shelley Zaragoza, Wanda J. Taylor, William Rittase, Nathan Suuremeyer, Liqiong Zhang and Robert Belliveau. *Paleoseismicity of the California Wash Fault, Southern Nevada*. Rep. no. 256-10. 7th ed. Vol. 37. Geological Society of America, 2005. Ser. 559. *Geological Society of America*. 19 Oct. 2005. Web. 1 May 2011. <http:// gsa.confex.com/gsa/2005AM/finalprogram/abstract_95950.htm>.